Spectroscopic properties and energy transfer parameters of Tm^{3+} ions in gallium lanthanum sulfide glass

2002 J. Phys.: Condens. Matter 14 9495

(http://iopscience.iop.org/0953-8984/14/41/307)

INSTITUTE OF PHYSICS PUBLISHING JOURNAL OF PHYSICS: CONDENSED MATTER

J. Phys.: Condens. Matter **14** (2002) 9495–9505 PII: S0953-8984(02)36368-9

Spectroscopic properties and energy transfer parameters of Tm^{3+} ions in gallium lanthanum sulfide glass

A S S de Camargo[1,3], S L de Oliveira[1], D F de Sousa[1], L A O Nunes[1] and D W Hewak[2]

[1] Instituto de Física de São Carlos, Universidade de São Paulo, CP 369, São Carlos-SP, 13566-590, Brazil
[2] Optoelectronics Research Center, University of Southampton, Southampton SO17 1BJ, UK

E-mail: andreasc@if.sc.usp.br

Received 29 April 2002, in final form 3 July 2002
Published 4 October 2002
Online at stacks.iop.org/JPhysCM/14/9495

Abstract

This work presents the spectroscopic characterization of Tm^{3+} doped gallium lanthanum sulfide (GaLaS) chalcogenide glass through absorption, fluorescence and lifetime measurements of excited $^3H_4$ and $^3F_4$ states, and a study of Tm^{3+}:Tm^{3+} energy transfer. The cross relaxation $^3H_4, {}^3H_6 \rightarrow {}^3F_4, {}^3F_4$ responsible for the pumping of level $^3F_4$ and the laser transition at 1800 nm ($^3F_4 \rightarrow {}^3H_6$), as well as the energy migration $^3H_4, {}^3H_6 \rightarrow {}^3H_4, {}^3H_6$ processes are studied in terms of the microscopic parameters of energy transfer C_{da} and C_{dd} obtained by the Kushida model of multipolar interactions and by a rate equation treatment of the dynamics of levels $^3F_4$ and $^3H_4$. From this treatment it was possible to simulate level $^3F_4$ temporal evolution curves for different Tm^{3+} concentrations, leading to results that are in excellent agreement with experimental ones. All the samples studied in the work present positive optical gain coefficients for excitation densities higher than 12 kW cm^{-2} indicating the potentiality of GaLaS:Tm^{3+} glass as a mid-infrared laser active medium.

1. Introduction

Technological interest has been demonstrated for Tm^{3+} doped crystals and glasses due to their potential use as laser active media, with emissions in the visible and mid-infrared spectral regions, for optical reading and atmospheric sensing applications. Other possible applications include medical diagnostics, use in optical radar, remote control and molecular spectroscopy [1–3]. One of the useful Tm^{3+} emissions in the mid-IR region is at 1800 nm ($^3F_4 \rightarrow {}^3H_6$ transition) that is usually achieved by the $^3H_4, {}^3H_6 \rightarrow {}^3F_4, {}^3F_4$ cross relaxation

[3] Author to whom any correspondence should be addressed.

pumping mechanism of level $^3F_4$, after exciting level $^3H_4$ at 800 nm. The advantage of this pumping mechanism for the Tm^{3+} laser is the ability to use commercially available and inexpensive diode lasers at 800 nm.

Among the suitable hosts for the investigation of rare-earth ion spectroscopic properties, sulfide glasses present very interesting characteristics such as low phonon energies, large refractive index and high covalence in bonding [4, 5]. Particularly, the gallium lanthanum sulfide glass (GaLaS) has been studied with Nd^{3+}, Er^{3+}, Pr^{3+}, Dy^{3+}, Tb^{3+}, Tm^{3+} and Ho^{3+} [1, 6–9] and it was the first chalcogenide glass fibre in which laser action was reported [10]. The GaLaS glass is non-toxic, non-hygroscopic, and presents high glass transition temperature (561 °C) making the glass fairly resistant to environmental effects and thermal damage that could be caused by the excitation with high power pump sources. Besides, it presents good visible and infrared transparency, high rare earth solubility, can be melted into bulk and pulled into fibre forms, and its low phonon energy ($\sim$425 cm^{-1}) reduces the probability of non-radiative losses [1].

The laser emission at 1800 nm is highly dependent on the efficiency of the energy transfer process among Tm^{3+} ions. Because level $^3F_4$ is pumped mainly by the cross relaxation $^3H_4$, $^3H_6 \rightarrow {}^3F_4$, $^3F_4$ involving two ions and also because such a process is favoured by the migration $^3H_4$, $^3H_6 \rightarrow {}^3H_4$, $^3H_6$ that spreads the excitation energy throughout the host [11] the study of these energy transfer mechanisms as well as the identification of the optimum ion density for maximum 1800 nm emission is of utmost importance in any attempt to build a Tm^{3+} based laser. Schweizer *et al* [9] have presented spectroscopic data on Tm^{3+} doped GaLaS and studied Tm^{3+}:Tb^{3+} energy transfer in codoped samples; however, no quantitative analysis of Tm^{3+}:Tm^{3+} energy transfer has been demonstrated, to the best of our knowledge. Therefore, in addition to the spectroscopic characterization of samples by absorption, fluorescence and lifetime measurements, this work presents a study of Tm^{3+}:Tm^{3+} energy transfer by analysing the dynamics of levels $^3H_4$ and $^3F_4$ using a rate equation formalism. The microscopic energy transfer parameters C_{da} and C_{dd} were calculated by the Kushida model [12] of multipolar interactions and from these values it was possible to obtain the W_{ET} macroscopic parameter as a function of Tm^{3+} concentration. Aiming to evaluate the validity of this parameter, its values were used in the rate equations for the calculation of level $^3H_4$ effective lifetimes ($\tau_{\mathrm{eff}}^{^3H_4}$), for the simulation of level $^3F_4$ temporal evolution and also to obtain steady state populations for optical gain calculations. It is worth noting that the calculation of these energy transfer parameters is a frequently used and important procedure when analysing the potentiality of a laser system.

2. Theory

2.1. Judd–Ofelt theory

The radiative properties of rare-earth ions in a variety of different host materials can be described by the Judd–Ofelt theory [13, 14]. This theory is well established in the literature and largely accepted; it allows the calculation of the intensity parameters Ω_λ by assuming the experimental and theoretical oscillator strengths are equal.

$$\frac{mc}{\pi e^2 N}\int \alpha(\nu)\,\mathrm{d}\nu = \frac{8\pi^2 m(n^2+2)^2}{27nh}\frac{\nu}{(2J+1)}\sum_{\lambda=2,4,6}\Omega_\lambda|\langle aJ|U^\lambda|bJ'\rangle|^2 \qquad (1)$$

where m is the electron mass, c is the speed of light, e is the electron charge, N is the number of ions per cm^3, $\int \alpha(\nu)\,\mathrm{d}\nu$ is the area of the absorption band, n is the refractive index, h is the Planck constant, ν is the transition frequency, J is the ground state quantum number

and $\langle aJ|U^{\lambda}|bJ'\rangle$ are the reduced matrix elements of the tensor operator U^{λ} of rank λ. From the obtainable Ω_{λ}, radiative properties such as transition rates, branching ratios, excited state lifetimes and quantum efficiencies can be calculated [8].

2.2. Energy transfer models

Regarding impurity ions in a host, several models can be used to describe non-radiative energy transfer among them [12, 15–17]. The Dexter model [15] for instance allows the calculation of the transfer probabilities in terms of the spectral overlap of the donor ion emission and acceptor ion absorption providing expressions for different coupling mechanisms, that is, dipole–dipole (dd) and dipole–quadrupole (dq). Even so, this model is most commonly applied to rare-earth ions for which the electronic transitions occur solely by dd interactions. However, for rare-earth ions such as Tm^{3+} in which transitions involved in the energy transfer are allowed by the electric quadrupole in addition to the forced electric dipole mechanism, higher order interaction mechanisms may become important when treating energy transfer and the use of the Dexter model is limited if the absorption and emission spectra result from the contribution of more than one mechanism.

In 1973, Kushida [12] proposed a model in which the calculations of the energy transfer probabilities P_{da} (da indicating donor–acceptor transfer) can be done separately for the dd, dq and quadrupole–quadrupole (qq) interactions by using the tensor operator method to calculate the microscopic parameter C_{da}. If the initial and final states of the interacting ions are the same, as is the case for the energy migration process $^3H_4$, $^3H_6 \rightarrow {}^3H_4$, $^3H_6$ in Tm^{3+} for example, the subscript da is substituted by dd (donor–donor). The expressions for C_{da} (or C_{dd}) are the following:

$$C_{da}^{dd} = \left(\frac{2}{3}\right)\frac{2\pi e^4}{\hbar(2J_d+1)(2J_a+1)}\left[\sum_{\lambda=2,4,6}\Omega_{d\lambda}\langle J_d|U^{\lambda}|J_d\rangle^2\right]\left[\sum_{\lambda=2,4,6}\Omega_{a\lambda}\langle J_a|U^{\lambda}|J_a\rangle^2\right]S, \tag{2}$$

$$C_{da}^{dq} = \frac{2\pi e^4\langle 4f|r_a^2|4f\rangle^2}{\hbar(2J_d+1)(2J_a+1)}\langle f\|C^2\|f\rangle^2\langle J_a\|U^{(2)}\|J_a\rangle^2\sum_{\lambda=2,4,6}\Omega_{d\lambda}\langle J_d\|U^{(\lambda)}\|J_d\rangle^2 S, \tag{3}$$

$$C_{da}^{qq} = \left(\frac{14}{5}\right)\frac{2\pi e^4\langle 4f|r_a^2|4f\rangle^2\langle 4f|r_d^2|4f\rangle^2}{\hbar(2J_d+1)(2J_a+1)}\langle f\|C^2\|f\rangle^4\langle J_d\|U_d^{(2)}\|J_d\rangle^2\langle J_a\|U_a^{(2)}\|J_a\rangle^2 S, \tag{4}$$

where J_a (J_d) is the total angular momentum of the acceptor (donor) ion starting level; $\Omega_{d\lambda}$ are the Judd–Ofelt [13, 14] intensity parameters for the donor ion; $\langle\|U^{(\lambda)}\|\rangle$ are the reduced matrix elements for the given transition of the donor ion; $\langle 4f|r_a^2|4f\rangle^2$ is the radial integral of the acceptor ion [18]; $\langle f\|C^2\|f\rangle = \sqrt{1.87}$ and S is the integral overlap between donor ion emission and acceptor ion absorption [11]. The superscripts dd, dq and qq stand for dipole–dipole, dipole–quadrupole and quadrupole–quadrupole interactions.

The energy transfer probability $P_{da}^{(s)}$ ($P_{dd}^{(s)}$) is then described as

$$P_{da}^{(s)} = \frac{C_{da}^{(s)}}{R^n}, \tag{5}$$

where s denotes the interaction mechanism (dd, dq or qq), n can assume the values of 6, 8 or 10 depending on the multipole order of interaction and R is the average distance between two interacting ions given by $R = (3/(4\pi N))^{1/3}$ where N is the density of ions.

The microscopic parameters C_{da} and C_{dd} can be used to obtain the previously mentioned W_{ET} macroscopic parameter, that, in the rate equations, is related to the cross relaxation and energy migration from level $^3H_4$. The expressions for calculating it depend on the energy migration regime (diffusion limited energy transfer [17] or hopping model [19]) and also

on the multipole order of interaction. Having previously concluded [11] that for Tm^{3+} ions higher order interaction mechanisms than dd should be taken into account, de Sousa *et al* [20] have also obtained the expressions of W_{ET} for dq and qq orders using both models. In such work, it was also verified that the diffusion limited regime is not valid for the Tm^{3+} doped fluoroindogallate glass, and experimental evidence indicates that this is the case for GaLaS as well. The expression for W_{ET} in the hopping model is then described by the sum $W_{ET}^{total} = W_{ET}^{dd} + W_{ET}^{dq} + W_{ET}^{qq}$ where the expressions for the terms are

$$W_{ET}^{dd} = 13(C_{da}^{dd})^{1/2}(C_{dd}^{dd})^{1/2}n_d, \tag{6}$$

$$W_{ET}^{dq} = 21(C_{da}^{dq})^{3/8}(C_{dd}^{dq})^{5/8}n_d^{5/3}, \tag{7}$$

$$W_{ET}^{qq} = 42(C_{da}^{qq})^{3/10}(C_{dd}^{qq})^{7/10}n_d^{7/3}, \tag{8}$$

n_d being the donor ion density.

2.3. Rate equations applied to Tm^{3+}

An effective way to describe the dynamics of a given energy level or a set of them is by using rate equations [20]. As concerns the present work, the rate equation system also serves as a tool to check the validity of the calculated values of W_{ET} and consequently C_{da} and C_{dd}, as will be discussed later. Figure 1 presents the partial energy level diagram of Tm^{3+} indicating the processes of cross relaxation (CR) and energy migration (EM) involving levels $^3H_6$ (n_0), $^3F_4$ (n_1) and $^3H_4$ (n_2). Based on such a scheme the following rate equations can be written:

$$\frac{dn_0}{dt} = -Rn_0 - W_{ET}n_2n_0 + n_2W_{20} + n_1W_{10}, \tag{9}$$

$$\frac{dn_1}{dt} = 2W_{ET}n_2n_0 + n_2W_{21} - n_1W_{10}, \tag{10}$$

$$\frac{dn_2}{dt} = Rn_0 - W_{ET}n_2n_0 - n_2W_{20} - n_2W_{21}, \tag{11}$$

where n_0, n_1 and n_2 represent the populations of levels $^3H_6$, $^3F_4$ and $^3H_4$ respectively, W_{ij} is the transition rate from level i to level j, W_{ET} is the energy transfer macro-parameter given in $cm^3\ s^{-1}$ and $R = \sigma I/h\upsilon$ is the pumping rate (σ being the absorption cross section at the pumping energy $h\nu$ and I the intensity of the pump light).

The influence of the energy transfer on the average $1/e$ lifetime of level $^3H_4$ can be evaluated by solving equations (9)–(11). Assuming low excitation density, n_0 is taken as constant and can be approximated to the total concentration n_t. For level $^3H_4$ (n_2) equation (11) takes the form

$$\frac{dn_2}{dt} = Rn_t - n_2\left(\frac{1}{\tau_0^{n_2}} + W_{ET}n_t\right) = Rn_t - \frac{n_2}{\tau_{\text{eff}}^{n_2}}, \tag{12}$$

where $(1/\tau_0^{n_2}) = W_{21} + W_{20}$ is the radiative decay rate of level $^3H_4$ in the absence of energy transfer, as is the case for low concentration samples, and $\tau_{\text{eff}}^{n_2}$ is the effective lifetime of level $^3H_4$ ($\tau_{\text{eff}}^{^3H_4}$) that depends on the radiative and non-radiative decay probabilities,

$$\frac{1}{\tau_{\text{eff}}^{n_2}} = \frac{1 + W_{ET}n_t\tau_0^{n_2}}{\tau_0^{n_2}}. \tag{13}$$

As can be seen, by introducing the values of W_{ET}^{total} in expression (13) it is possible to calculate level $^3H_4$ effective lifetimes ($\tau_{\text{eff}}^{^3H_4}$) as a function of Tm^{3+} concentration and compare these values with the experimentally obtained ones. Moreover, an analysis of the time evolution

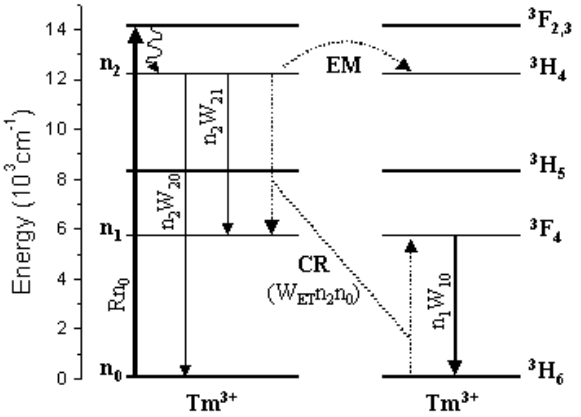

Figure 1. Partial energy level diagram of Tm^{3+} in GaLaS glass. The processes of cross relaxation (CR) and energy migration (EM) are indicated in addition to those corresponding to the terms that compose the rate equations.

of the level $^3F_4$ population can be done using the W_{ET}^{total} and $\tau_{\text{eff}}^{^3H_4}$ values. The solution for this level, in a pulsed regime, is

$$n_1(t) = \frac{n_2(0)(2W_{ET}n_t + W_{21})}{W_{10} - (\tau_{\text{eff}}^{n_2})^{-1}}\left(\exp\left(-\frac{t}{\tau_{\text{eff}}^{n_2}}\right) - \exp(-W_{10}t)\right), \tag{14}$$

where W_{10} and W_{21} are the $^3F_4 \rightarrow {}^3H_6$ and $^3H_4 \rightarrow {}^3H_6$ decay rates.

3. Experimental details

The GaLaS bulk glass samples with composition 65% Ga_2S_3, 33% La_2S_3 e 2.0% La_2O_3 doped with the nominal concentrations of 0.1; 1.0; 2.0; 4.0 and 6.0 wt% Tm_2S_3, were obtained by melt quenching the raw materials after heating them for 24 h at 1150 °C. The real concentration of Tm^{3+} ions was determined by EDX measurements using a digital microscope and the Link Analytical QX2000 software. The samples were cut, optically polished and characterized by absorption from 500 to 2100 nm, using a Perkin Elmer Lambda 900 spectrophotometer, and by fluorescence using a krypton ion laser with $\lambda_{exc} = 647$ nm. The fluorescence was filtered from 750 to 2200 nm by a 0.3 m monochromator, collected by an InAs photodetector and amplified by a lock-in. Lifetime values of $^3H_4$ and $^3F_4$ excited states were obtained from the fluorescence decay curves corresponding to transitions $^3H_4 \rightarrow {}^3H_6$ and $^3F_4 \rightarrow {}^3H_6$ using as excitation sources at 650 nm either a chopper modulated dye laser (for the samples with less than 2.0 wt% Tm_2S_3), or an OPO laser. The fluorescent signals were collected by either the InAs detector or a photomultiplier tube and registered by a digital oscilloscope. The spectroscopic measurements were all made at room temperature.

4. Results

The ground state absorption spectrum of GaLaS:Tm^{3+} (2.0 wt%) is presented in figure 2 and it is representative for all samples. Since the optical absorption edge of the glass starts at around 600 nm, the spectrum displays only five characteristic Tm^{3+} bands in the range of 500–2100 nm as indicated. Figure 3 presents the emission spectra of the GaLaS samples doped with 0.1 and 6.0 wt% Tm_2S_3 in the region of 700–2200 nm. The characteristic transitions are indicated,

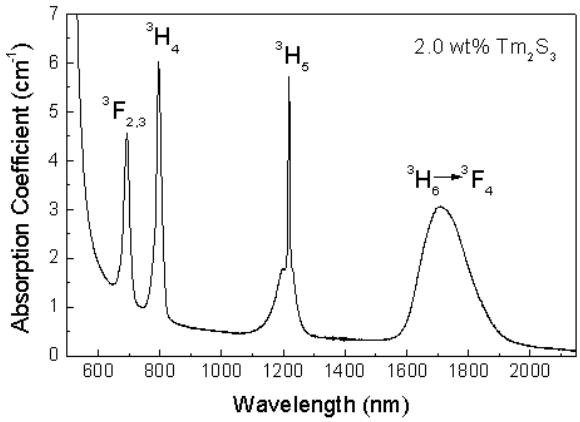

Figure 2. Representative ground state ($^3H_6$) absorption spectrum of GaLaS sample doped with 2.0 wt% Tm_2S_3 obtained at $T = 300$ K.

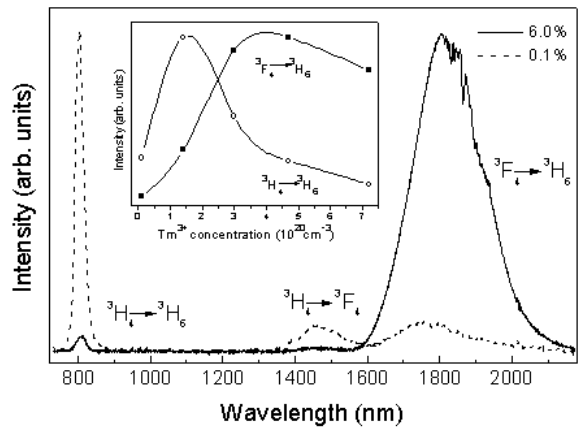

Figure 3. Emission spectra of GaLaS samples doped with 0.1 and 6.0 wt% Tm_2S_3 obtained with excitation at 647 nm at $T = 300$ K. The inset of the figure presents the intensities of the bands corresponding to $^3H_4 \rightarrow {}^3H_6$ and $^3F_4 \rightarrow {}^3H_6$ transitions as a function of Tm^{3+} ion density.

and as can be seen the intensity ratio of the bands at 800 and 1800 nm practically inverts when the concentration is increased from 0.1 to 6.0 wt%. The intensities of these bands as a function of Tm^{3+} densities are shown in the inset of the figure. From the absorption and emission spectra, the experimental oscillator strengths and emission energies were obtained for the 2.0 wt% Tm_2S_3 doped sample, and using the Judd–Ofelt theory [13, 14] Ω_2, Ω_4 and Ω_6 intensity parameters were calculated. They were then used for the calculation of transition probabilities W, branching ratios β and radiative lifetimes τ_0 of levels $^3H_4$ and $^3F_4$ which values are all listed in table 1.

Table 2 gives the values of the energy transfer microscopic parameters C_{dd} and C_{da} calculated by using the values of Ω_λ presented in table 1, in expressions (2)–(4) for different interaction mechanisms.

The obtained C_{dd} and C_{da} were then used in expressions (6)–(8) to obtain the W_{ET} parameters presented in table 3 as a function of Tm^{3+} density. Once the values of W_{ET} were

Table 1. Intensity parameters Ω_λ, and radiative properties of Tm^{3+} in GaLaS glass.

Transition ($J \rightarrow J'$)	Peak position (cm^{-1})	$W_{JJ'}$ (s^{-1})	$\beta_{JJ'}$ (JO)	$\beta_{JJ'}$ (exp)	τ_0 (μs)
$^3H_4 \rightarrow {}^3H_6$	12 379	5614	0.902	0.692	160
$^3H_4 \rightarrow {}^3F_4$	6 900	518	0.083	0.308	$\eta = 98\%$
$^3H_4 \rightarrow {}^3H_5$	4 350	92.4	0.015	—	
$^3F_4 \rightarrow {}^3H_6$	5 583	1041	1	1	960

$\Omega_2 = 5.8 \times 10^{-20}$ cm^2 $\Omega_4 = 1.6 \times 10^{-20}$ cm^2 $\Omega_6 = 1.3 \times 10^{-20}$ cm^2
$\text{rms}_{error} = 5.0\%$ $n = 2.4$

Table 2. Energy transfer microscopic parameters for different interaction mechanisms.

Interaction	Tm^{3+}–Tm^{3+} energy transfer micro-parameters	
mechanism	C_{da} (cross relaxation)	C_{dd} (energy migration)
dd (cm^6 s^{-1})	1.27×10^{-40}	59.2×10^{-40}
dq (cm^8 s^{-1})	1.88×10^{-54}	77.5×10^{-54}
qq (cm^{10} s^{-1})	4.66×10^{-68}	189×10^{-68}

Table 3. Experimental lifetime values of Tm^{3+} $^3H_4$ and $^3F_4$ excited states and effective lifetimes of $^3H_4$ obtained from the calculated W_{ET}^{total} values of all samples.

Tm_2S_3 (wt%)	Tm^{3+} density (10^{20} cm^{-3})	W_{ET}^{total} (10^{-16} cm^3 s^{-1})	$^3H_4$ τ_{eff} (μs)	$^3H_4$ τ_{exp} (μs)	$^3F_4$ τ_{exp} (μs)
0.1	0.8	0.02	156	150	1040
1.0	1.8	0.09	127	124	950
2.0	3.4	0.31	60	60	910
4.0	5.3	0.8	20	21	460
6.0	7.2	1.52	9	9	300

introduced in equation (13), it was possible to get $\tau_{\text{eff}}^{^3H_4}$ and compare the results with the experimental ones taken from level $^3H_4$ decay curves when the intensity has the approximate value of $1/e$. The $1/e$ lifetime values of level $^3F_4$ were also obtained from its decay curves. Results are all in table 3.

5. Discussions

5.1. Spectroscopic results

Regarding the ground state absorption spectra of GaLaS:Tm^{3+} in figure 2, the band lineshapes and energies are very similar to those observed for Tm^{3+} in other chalcogenide glasses [21, 22] and identical to previous results on GaLaS:Tm^{3+} [9]. The line strengths of transitions in GaLaS:Tm^{3+} are large due to the large covalence of the glass bonds and high refractive index. The UV absorption edge of the host, starting at around 600 nm, superposes with the ion higher energy levels $^1G_4$, $^1D_2$ etc, and the multiphonon absorption edge in the IR (not shown) starts at around 7500 nm. For the Judd–Ofelt calculations, closely spaced $^3F_2$ and $^3F_3$ levels were treated as one and, for the $^3H_6 \rightarrow {}^3H_5$ transition, the contribution of the magnetic dipole interaction was taken into account. The values of $\Omega_2 = 5.8 \times 10^{-20}$ cm^2, $\Omega_4 = 1.6 \times 10^{-20}$ cm^2 and $\Omega_6 = 1.3 \times 10^{-20}$ cm^2 are also in excellent agreement with previous data [9]. As

a consequence of large oscillator strengths, the intensity parameters of lanthanide ions are higher in chalcogenides than in other glasses. Actually, the high covalence and low phonon energy of these glasses generate transition probabilities about ten times larger than in fluoride glasses [23]. The host's high covalence character is also evidenced by the large Ω_2 value when compared to Ω_4 and Ω_6. Due to low phonon energy and large energy gap (4360 cm^{-1}) between $^3H_4$ and the lower lying $^3H_5$ levels, the quantum efficiency $\eta = \tau_{meas.}/\tau_0$ of level $^3H_4$ ($\tau_{meas.}$ is the experimental lifetime) for the 0.1 wt% doped sample is 98% as indicated in table 1.

In the emission spectra of figure 3, the intensity inversion of the bands at 1800 and 800 nm as the concentration is increased from 0.1 to 6.0 wt% is attributed to an increase in the cross relaxation probability which causes an increase of the population of level $^3F_4$ while decreasing that of $^3H_4$. This behaviour becomes very clear analysing the curves in the inset of figure 3. Note that the intensity of the band at 800 nm ($^3H_4 \rightarrow {}^3H_6$ transition) drastically decreases for concentrations higher than 1.0 wt% (1.8×10^{20} Tm^{3+} ions cm^{-3}), which is due to the increase in the cross relaxation that, as a consequence, causes a progressive increase in the intensities of the curve corresponding to the 1800 nm band. By examining these curves it is possible to see that the sample presenting higher cross relaxation efficiency in the set studied is the one doped with 4.0 wt% Tm_2S_3 (5.3×10^{20} Tm^{3+} ions cm^{-3}). For 6.0 wt% doping however, there is a decrease in intensity probably due to the $^3F_4$, $^3H_6 \rightarrow {}^3F_4$, $^3H_6$ energy migration between Tm^{3+} ions followed by transfer to an impurity or due to the inverse cross relaxation $^3F_4$, $^3F_4 \rightarrow {}^3H_4$, $^3H_6$.

The effect of increasing cross relaxation can also be proved from the decrease in lifetimes of level $^3H_4$ as the doping concentration increases. The experimental $1/e$ lifetime values listed in table 3 were taken from decay curves which, except for the 0.1 wt% doped sample, are all non-exponential due to CR. The curves corresponding to level $^3F_4$ however, are all exponential. For low Tm^{3+} ion density the decay is mainly radiative and that results in longer lifetime values but as the concentration increases other interactions between Tm^{3+} ions such as energy migration followed by transfer to an impurity become possible, and that causes a progressive decrease of the lifetimes as can be seen in table 3.

5.2. Energy transfer and rate equations

Similarly to what is observed for Tm^{3+} doped fluoroindogallate glasses [11], the values of C_{dd} listed in table 2 are larger than those of C_{da} indicating a strong probability of energy migration within level $^3H_4$. Besides, the values of C_{dd} in GaLaS are much larger than in the fluoroindogallate host as expected due to higher Tm^{3+} emission and absorption cross sections. The C_{da} parameter values, however, are a little higher in the fluoroindogallate host [20] and that can be understood if one considers that, because the cross relaxation is a non-resonant (phonon dependent) process and the energy difference between $^3H_4 \rightarrow {}^3H_6$ and $^3H_6 \rightarrow {}^3F_4$ emission and absorption bands is larger in GaLaS than in the fluoride glass, a larger number of phonons have to be taken into account in GaLaS than in the fluoride glass so that the spectral overlap is appreciable.

To indirectly verify the validity of calculated macroscopic and microscopic parameters, the W_{ET} values in table 3 were used to obtain the effective lifetime values of level $^3H_4$ ($\tau_{\mathrm{eff}}^{^3H_4}$). The results are also presented in table 3, and as can be seen they are in very good agreement with the experimentally taken $1/e$ values. Moreover, by using the obtained W_{ET} and $\tau_{\mathrm{eff}}^{^3H_4}$ values as a function of Tm^{3+} concentration to solve equations (9)–(11), we were able to perform very successful simulations of the level $^3F_4$ population rise in time (equation (14)) which is proportional to its luminescence intensity curve in time. Figure 4 gives the rise curves in detail (open circles) and the simulations (solid curves) obtained using equation (14) for the samples

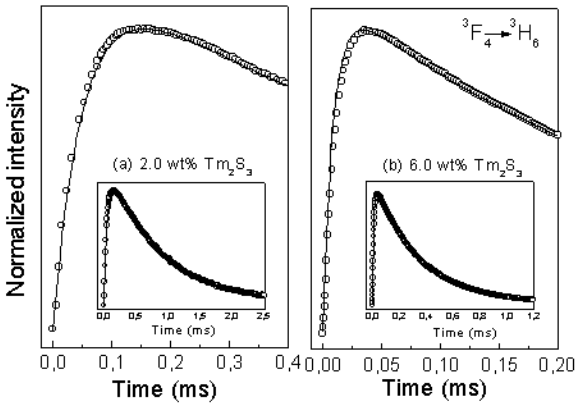

Figure 4. Temporal evolution curves of the level $^3F_4$ population for the (a) 2.0 wt% and (b) 6.0 wt% Tm_2S_3 doped GaLaS samples. Open circles correspond to the experimental data and solid curves are those obtained from the rate equation simulations. The insets present the complete rise and decay ranges of the curves and simulations.

doped with 2.0 and 6.0 wt%. The inset presents the complete curves, that is, including the decay range of time. Note that when the Tm^{3+} concentration increases, and consequently W_{ET}, the sample rise times become shorter as well as their decay times as previously discussed.

The good results obtained up to this point were enough to validate the values of W_{ET}, C_{da} and C_{dd} but we were also able to evaluate W_{ET} values by calculating the optical gain profiles of the transition $^3F_4 \rightarrow {}^3H_6$ at 1800 nm. For these calculations, the steady state populations of levels $^3F_4$ and $^3H_6$ were obtained by solving the rate equations for a continuous pumping, employing the values of W_{ET} and $\tau_{\mathrm{eff}}^{^3H_4}$. Figure 5 presents the optical gain coefficient ($G(\lambda)$) curves as a function of excitation and Tm^{3+} ion densities. All the samples in the set studied presented positive gain and from the profiles it was verified that for excitation densities higher than 12 kW cm^{-2} the sample that presents higher, positive gain is the one doped with 6.0 wt% Tm_2S_3. For lower densities however, the optimum concentration is about 4.0 wt% (5.3×10^{20} ions cm^{-3}), and the curves reproduce the one shown in the inset of figure 3 for the intensity behaviour of transition $^3F_4 \rightarrow {}^3H_6$, very well. From the curves shown in figure 5, $G(\lambda)$ values of 6.0 and 4.0 wt% Tm_2S_3 are 2.1 cm^{-1} ($I = 20$ kW cm^{-2}) and 0.83 cm^{-1} ($I = 8$ kW cm^{-2}) respectively. The observation of positive gain corroborates with the primary conclusion [9] that GaLaS:Tm^{3+} is a promising material for mid-infrared laser media.

6. Conclusions

GaLaS:Tm^{3+} glass samples were characterized by optical spectroscopy and present the typical absorption and fluorescence bands of Tm^{3+} in the near infrared and visible spectral regions. The intensity parameters and radiative properties were obtained by the Judd–Ofelt theory and are practically identical to those presented in the literature for GaLaS:Tm^{3+} glass. The microscopic parameters C_{dd} and C_{da} associated with the energy transfer processes of energy migration and cross relaxation were obtained taking into account dd and higher order interaction mechanisms using the Kushida model. These parameters were used to calculate the values of the macroscopic parameter W_{ET} and using the last it was possible to obtain the effective lifetime values of level $^3H_4$ in very good agreement with experimental data. Moreover, the values of W_{ET} and $\tau_{\mathrm{eff}}^{^3H_4}$ were applied in the simulations of level $^3F_4$ temporal evolution as a

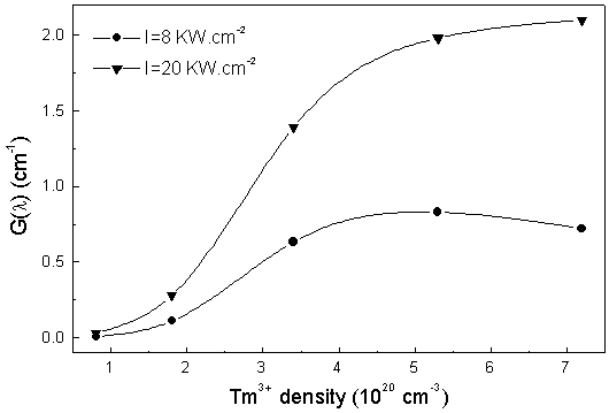

Figure 5. Optical gain coefficients $G(\lambda)$, as a function of Tm^{3+} ion density for excitation densities of 8 and 20 kW cm^{-2}.

function of Tm^{3+} concentration. The good agreement between experimental and calculated curves gives credit to the C_{dd} and C_{da} microscopic parameters calculated taking into account higher than dd order interaction mechanisms. Finally, the ability to obtain positive optical gain in all samples using the calculated W_{ET} values in the calculation of the steady state populations also points out the reliability of these parameter and indicates the potentiality of GaLaS:Tm^{3+} as a laser medium at 1800 nm.

Acknowledgments

This work was supported by FAPESP (Fundação de Amparo a Pesquisa do Estado de São Paulo) and by CNPq (Conselho Nacional de Desenvolvimento Científico e Tecnológico). Thanks to Jacob Smith from the Optoelectronics Research Centre at the University of Southampton for helping with the preparation of the samples.

References

[1] Schweizer T, Samson B N, Hector J R, Brocklesby W S, Hewak D W and Payne D N 1999 *Infrared Phys. Technol.* **40** 329
[2] Kaufman R, Hartmann A and Hibst R 1994 *J. Dermatol. Surg. Oncol.* **20** 112
[3] Miazato K, de Sousa D F, Delben A, Delben J R, de Oliveira S L and Nunes L A O 2000 *J. Non-Cryst. Solids* **273** 246
[4] Kumpta P N and Risbud S H 1994 *J. Mater. Sci.* **29** 1135
[5] Schweizer T, Hewak D W, Payne D N, Jensen T and Huber G 1996 *Electron. Lett.* **32** 666
[6] Ye C C, Hewak D W, Hempstead M, Samson B N and Payne D N 1996 *J. Non-Cryst. Solids* **208** 56
[7] Schweizer T, Hewak D W, Samson B N and Payne D N 1997 *J. Lumin.* **419** 72
[8] Lima S M, Sampaio J A, Catunda T, de Camargo A S S, Nunes L A O, Baesso M L and Hewak D W 2001 *J. Non-Cryst. Solids* **284** 274
[9] Schweizer T, Samson B N, Hector J R, Brocklesby W S, Hewak D W and Payne D N 1999 *J. Opt. Soc. Am.* B **16** 308
[10] Schweizer T, Samson B N, Moore R C, Hewak D W and Payne D N 1997 *Electron. Lett.* **33** 414
[11] de Sousa D F, Lebullenger R, Hernandes A C and Nunes L A O 2002 Evidence of higher order mechanisms than dipole–dipole interactions in the $Tm^{3+} \rightarrow Tm^{3+}$ energy transfer in fluoroindogallate glasses *Phys. Rev.* B **65** 094204
[12] Kushida T 1973 *J. Phys. Soc. Japan* **34** 1318
[13] Judd B R 1962 *Phys. Rev.* **127** 750

[14] Ofelt G S 1962 *J. Chem. Phys.* **37** 511
[15] Dexter D L 1953 *J. Chem. Phys.* **21** 836
[16] Miyakawa T and Dexter D L 1970 *Phys. Rev.* B **1** 2961
[17] Yokota M and Tanimoto F J 1967 *J. Phys. Soc. Japan* **22** 779
[18] Rajnak K 1962 *J. Chem. Phys.* **37** 2440
[19] Burshtein A I 1972 *Sov. Phys.–JETP* **35** 882
[20] de Sousa D F, Lebullenger R, Hernandes A C and Nunes L A O 2002 Microscopic and macroscopic parameters of energy transfer between Tm^{3+} ions in fluoroindogallate glasses *Phys. Rev.* B **66** 024207
[21] Kadono K, Yazawa T, Shojiya M and Kawamoto Y 2000 *J. Non-Cryst. Solids* **274** 75
[22] Shin Y B, Cho W Y and Heo J 1996 *J. Non-Cryst. Solids* **208** 29
[23] Ye C C, Petrin R R, Sibley W A, Madigou V, Adam J L and Suscavage M J 1989 *Phys. Rev.* B **39** 80
[24] Subramanyam Y, Moorthy L R and Lakshman S V J 1992 *J. Non-Cryst. Solids* **139** 67